

Industrial n-type solar cells: Towards 20% efficiency

Ingrid Romijn, ECN Solar Energy, Petten, The Netherlands, Lang Fang, Yingli Solar, Baoding, China, & Ard Vlooswijk, Tempres Systems BV, Vaassen, The Netherlands

Fab & Facilities

Materials

Cell Processing

Thin Film

PV Modules

Power Generation

Market Watch

ABSTRACT

This paper presents examples of recent process developments at ECN in silicon solar cells on n-type monocrystalline base material. For all PV manufacturers, the challenge is to increase module efficiencies while maintaining low production cost. An effective way to move to higher and more stable efficiencies, using low-cost industrial-type processing, is n-type solar cell technology. The solar cell considered in this paper is the n-pasha cell – a bifacial solar cell with homogeneous diffusions and screen-printed metallization. The n-pasha cell is currently produced on an industrial scale by Yingli Solar; in 2011 a maximum solar cell conversion efficiency of 19.97% was obtained using this cell concept on 239cm² n-type Cz at the ECN laboratory. The focus of the paper will be increasing efficiency by optimization of the cell process, in particular the front-side metallization, and by improvements to the rear-surface passivation. These two steps have contributed to an increase in efficiency of 0.8%, allowing cell efficiencies of 20% to be reached.

n-type silicon solar cells

More than 85% of the solar cells currently produced worldwide make use of crystalline silicon, and most are based on p-type wafers [1]. The most common multi- and monocrystalline solar cells used in the majority (~90%) of PV modules are made by applying a phosphorous-diffused emitter and an aluminium back-surface field to a p-type wafer. Efficiencies obtained are of the order of 17% and 18%, respectively, for multicrystalline and monocrystalline p-type wafers. Sunpower and Sanyo use n-type wafers as base material for their high-efficiency cells: interdigitated back-contacted (IBC) cells in the case of Sunpower [2], and heterojunction with intrinsic thin (HIT) layer cells in the case of Sanyo [3]. Efficiencies above 23% have been reported with both cell types [4]. Yingli Solar also took high-efficiency cells based on n-type wafers into mass production in 2010, under the type name 'PANDA' and average efficiencies of about 18.9% were achieved in their production in 2011 [5].

The use of n-type material has several advantages over the use of p-type. First, there is no boron dopant in n-type material; hence formation of boron-oxygen (B-O) complexes will be negligible [6]. B-O complexes are formed upon exposure to light in p-Cz material that is relatively rich in oxygen, and degrade the bulk lifetime of the material. This severely limits the efficiencies that can be obtained with these wafers [7,8]. Second, n-type material has been found to be much less sensitive to transition metal impurities such as, for example, Fe [9]. This could give the n-type material a higher tolerance for variations in the feedstock purity [10].

Manufacturing solar cells based on n-type wafers poses some additional challenges compared to the processing

of p-type material. For n-type cells, boron emitter diffusion requires higher temperatures than phosphorous emitter diffusions common to p-type cells. Furthermore, in 'standard' p-type cells, the p⁺ back-surface field (BSF) is formed by alloying the aluminium back side, while in n-type cells the n⁺ BSF is usually a phosphorous diffusion. Formation of good emitter and BSF for n-type cells is therefore a challenge. In addition, the conventional method of passivating the emitter by silicon nitride (SiN_x) is less effective on the p⁺ boron emitter [11]. Several methods have recently become available to passivate boron emitters effectively at relatively low temperatures. One that has received considerable attention is the application of an Al₂O₃ layer by atomic layer deposition (ALD). This layer introduces fixed negative charges at the Al₂O₃/Si interface [12,13]. ECN has developed a simple wet chemical process followed by a plasma-enhanced chemical vapour deposition (PECVD) that forms a SiO_x/SiN_x passivation stack on the boron emitter, having similar passivation performance to passivation by Al₂O₃ layers [14,15].

“The n-pasha cell has an open rear side and is therefore a bifacial cell, which produces additional power output when incorporated into a module with a transparent rear side.”

ECN's n-pasha cell concept

Fig. 1 shows the basic configuration of the n-pasha (passivated all sides H-pattern)

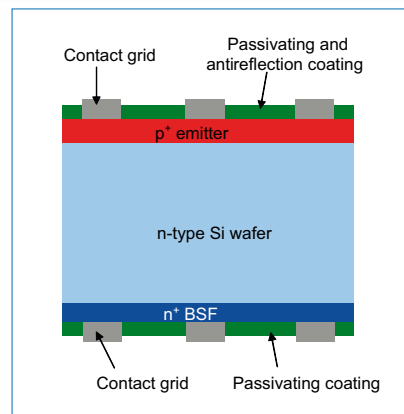


Figure 1. Cross section of the ECN n-pasha cell, featuring an n-type Cz Si wafer with a boron p⁺ emitter and phosphorous n⁺ BSF. Yingli's PANDA cells are also based on this structure.

solar cell. The n-pasha cell has an open rear side and is therefore a bifacial cell, which produces additional power output when incorporated into a module with a transparent rear side [15]. The bifacial characteristic distinguishes it both from conventional (full aluminium back side) p-type solar cells and from high-efficiency passivated emitter and rear contact (PERC) n-type or p-type cells. Bifacial cells benefit from enhanced internal reflection, which is better for a dielectric rear coating than for a full aluminium alloy at the rear. Both the front and rear sides of n-pasha cells feature H-grid metallization patterns; Yingli's PANDA cells are also based on this structure.

The n-pasha cells are fabricated on 6-inch semi-square n-type Cz wafers. The first processing step is to texture the wafers with random pyramids using alkaline etching. The boron emitter and phosphorous BSF are formed using an industrial tube furnace from Tempres

[16]. A 60Ω/sq emitter is made using BBr₃ as a precursor. The BSF is made using POCl₃ as a precursor and provides additional lateral conductivity at the rear side. This results in a good fill factor (*FF*) despite the open-rear-side metallization, even for cells processed on high-resistivity (~8Ωcm) base material.

The front and rear sides are both coated with SiN_x layers for passivation and antireflective purposes. The metallization is applied to both sides using screen printing, and the contacts on the emitter and BSF are formed during a single co-firing step. The front and rear metallization can be directly soldered, so no additional metallization step is necessary to allow interconnection into a module. The open rear side also ensures that there will be no bending of the cells when (very) thin wafers are used, as is the case for the full aluminium BSF on p-type cells. All processing steps used for the n-pasha cell are compatible with production on an industrial scale.

Industrialization of n-pasha

For industrialization, a cell concept needs to be applicable to material from different suppliers. At ECN several batches of standard n-pasha cells were processed from n-type Cz wafers from different commercial wafer producers. The base resistivity of the materials ranged from 1.5 to 10Ωcm. The efficiency distribution of n-pasha cells on material from five different wafer suppliers is shown in Fig. 2. The efficiencies obtained range from 19.0 to 19.4%, indicating that high-efficiency n-pasha cells can be made, with the efficiency being largely independent of the base material.

The n-pasha cell process has been developed in ECN's pilot line. In June 2009, ECN, Amtech Systems and Yingli Green Energy announced a three-party research agreement, to further develop and industrialize the n-type open-rear-side cell. The best independently confirmed (by ISE CalLab) efficiency of n-pasha cells processed in the Yingli cell line is 19.5% (on 239cm²) [5].

Efficiency improvements to n-pasha cells

During the early stages of development of the n-pasha concept at ECN, attention was mostly focused on optimizing the front and rear sides, i.e. the boron diffusion and the front- and rear-surface passivation [15,17,18]. In this paper the results of two recent efficiency enhancements for n-pasha cells will be presented. The first one is stencil printing of the front-side metallization (an option generically available to p-type as well as n-type solar cells); and the second is improved

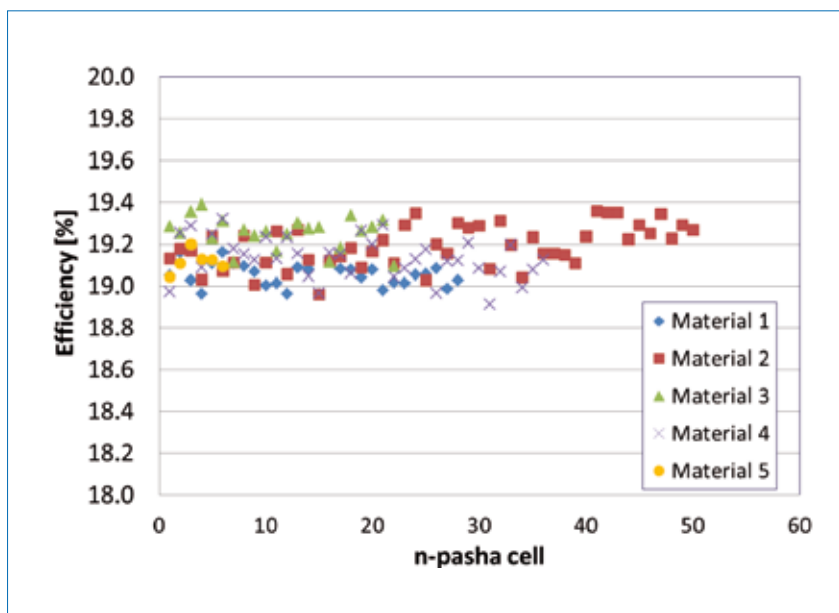


Figure 2. Efficiency distribution of n-pasha cells on Cz material from five different suppliers, with resistivity of the base material ranging from 1.5 to 10Ωcm. The index of the cells in each group is indicated on the x-axis. Efficiencies vary between 19.0 and 19.4%, indicating that high-efficiency n-pasha cells can be made with wafers from a variety of commercial material suppliers.

phosphorous BSF (specific to n-pasha cells).

Front-side metallization

Over the past years ECN has developed a two-step stencil-printing metallization [19]. By using a single-layer stencil and a high aspect ratio paste, the deposition of very high, fine lines has been demonstrated (see Fig. 3). However, the completely open nature of the fingers in the stencil requires a two-step process in which fingers are stencilled and busbars are printed separately.

Applying the two-step process to the n-pasha cells, 55μm-wide fingers with an aspect ratio of over 0.5 (height/width) have been achieved, as can be seen in Fig. 3. The metal coverage and therefore shading

of the front surface can be reduced from approximately 7.5% to 5.5%, i.e. by around 2%. The line definition is also much better using stencil printing (see Fig. 4).

A change of equipment is not required, but the metallization paste has to be optimized for stencil printing. The reduced metallization coverage will result in an increase in short-circuit current (*I_{sc}*) due to a larger active area of the solar cell, as well as a rise in open-circuit voltage (*V_{oc}*) due to the smaller contact area. The smaller contact area reduces the contribution of contact recombination to *J_{0front}*, resulting in an overall reduction of dark saturation current. The smaller contact area may result in a higher resistive loss due to contact resistance, but in our experience the area-specific contact resistance of

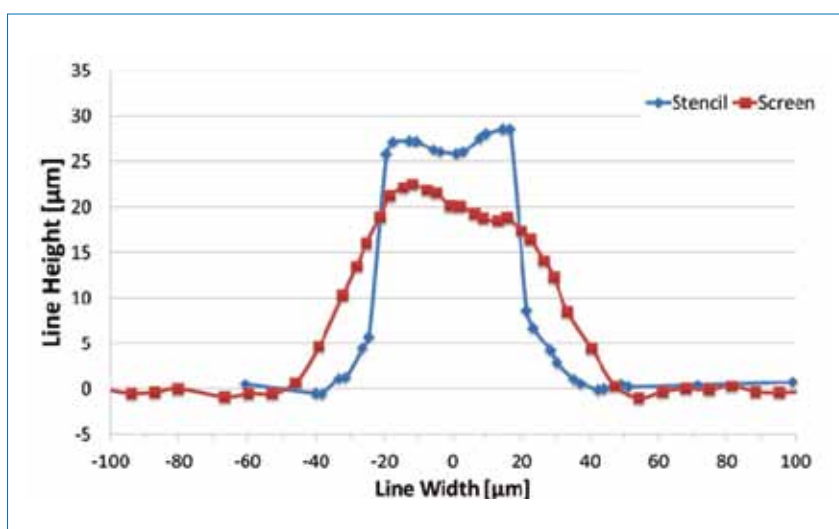


Figure 3. Measured cross sections of two metal fingers: deposited using screen printing (red) and deposited using stencilling (blue).

stencil-printed fine lines is slightly better than for screen-printed normal lines.

Several tests of stencil-printed front grids for n-pasha cells have been performed in order to investigate optimized pastes and tune the stencil parameters. The averaged I_{sc} and V_{oc} results from the most recent experiment between a group with a standard screen-printed and a stencil-printed front-side print are shown in Fig. 5. Because of the reduced metal coverage, the FF is reduced by approximately 0.5% relative for the stencil print due to increased line resistance (see Table 1). However, this is more than compensated for by the gain in I_{sc} and V_{oc} giving rise to an increase in efficiency of around 0.4% absolute.

“The resulting gain in efficiency using a stencil print is around 2% relative, which equates to an increase of almost 0.4% absolute for a 19% n-pasha cell.”

The relative gains in I_{sc} and V_{oc} and relative losses in FF for stencil print vs. screen print are summarized in Table 1 from three different experiments. The resulting gain in efficiency using a stencil print is around 2% relative, which equates to an increase of almost 0.4% absolute for a 19% n-pasha cell. An additional attractive feature of stencil printing is that the silver consumption can be reduced by 10 to 20% compared to (single print) screen printing.

Rear-surface passivation

The surface recombination of the non-metallized area on the rear surface depends on two factors: the surface doping concentration determined by the BSF diffusion, and the surface passivation by the deposited dielectric layer. The two are interrelated: a higher surface doping concentration typically results in higher recombination velocities at the interface with the dielectric layer. Moreover, Auger recombination takes place in the doped layer, which is proportional to the square of the doping concentration (in the appropriate low-level injection regime). Free carrier absorption also occurs in the doped layer, which will increase as doping increases. Generally, a lower surface doping concentration will result in higher J_{sc} and V_{oc} .

Two further constraints on the doping profile are: 1) the requirement for good contact resistance with the rear metallization; and 2) the requirement for sufficient lateral conductance between the metal fingers to ensure a high FF . An industrial optimization of all these effects is being pursued: as a first step, the phosphorous BSF profile has been optimized.

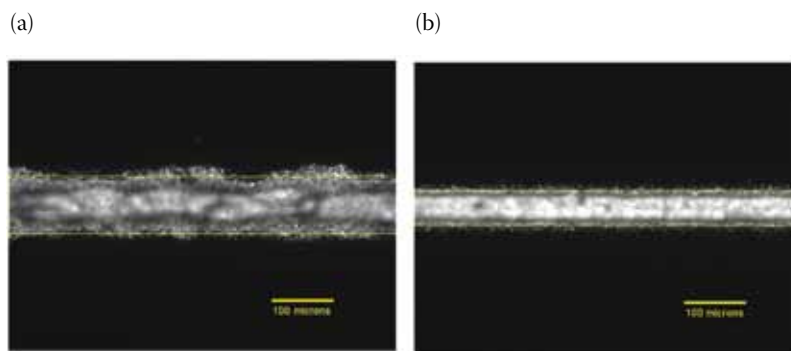


Figure 4. Microscope picture of (a) a screen-printed finger, and (b) a stencil-printed finger.

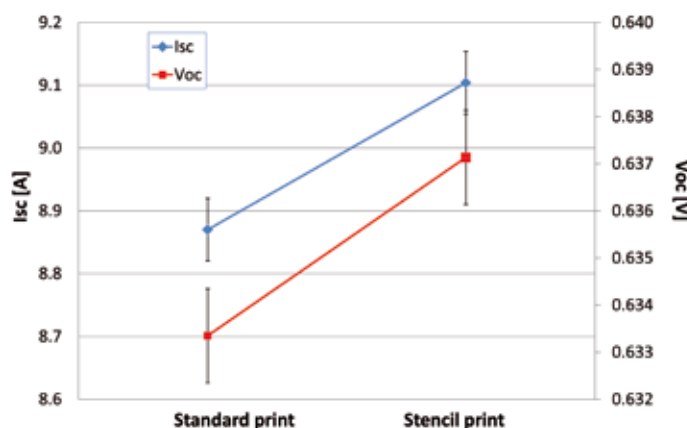


Figure 5. Averaged I_{sc} and V_{oc} values for groups of cells with a standard screen-printed front side and a stencilled front side.

	I_{sc} (%)	V_{oc} (%)	FF (%)	η (%)
Experiment 1	1.5	0.6	-0.4	1.9
Experiment 2	2.6	0.5	-0.9	2.2
Experiment 3	2.2	0.4	-0.3	2.3

Table 1. Relative changes in I - V characteristics for stencil print vs. screen print from three experiments.

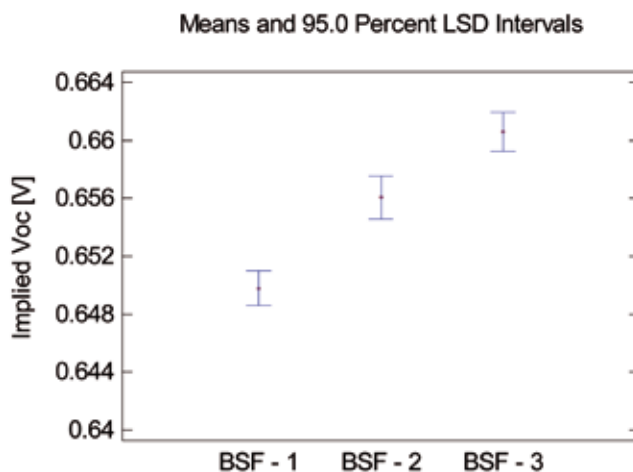


Figure 6. Implied V_{oc} values of cells for three different BSF profiles with increasing R_{sheet} .

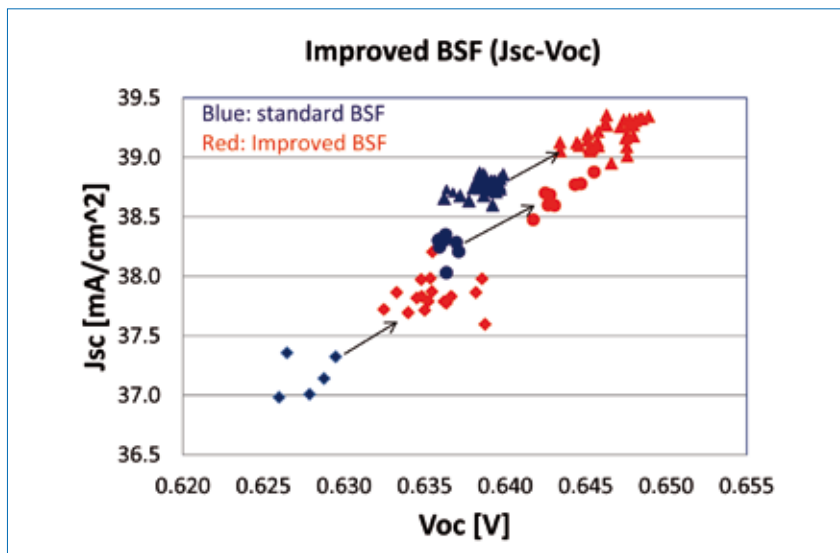


Figure 7. Current and voltage gains observed for experiment runs using a variety of base materials (represented by different symbols). The colours depict the type of BSF: blue for standard (BSF-1 in Fig. 6) and red for improved (BSF-3 in Fig. 6). The arrows are a guide for the eye to indicate the improvement within an experiment.

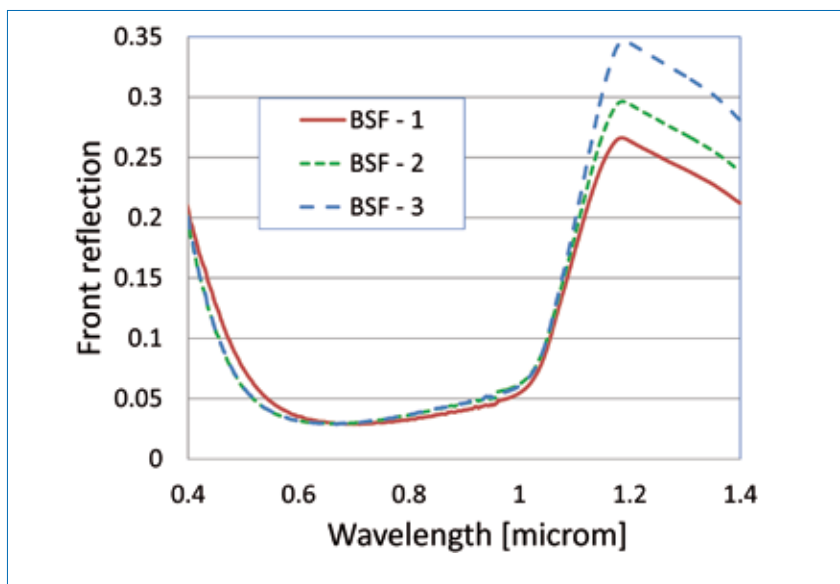


Figure 8. Front reflection measurements of cells with three different BSF profiles. Above 1000nm, the increase in reflection is clear, indicating a decrease in free-carrier absorption and an increase in internal rear reflection. This results in an increase in J_{sc} .

	I_{sc} [A]	J_{sc} [mA/cm ²]	V_{oc} [V]	FF [-]	η [%]
Group 1 (standard)					
avg	9.26	38.7	0.640	0.784	19.4
max	9.27	38.8	0.640	0.787	19.5
Group 2 (improved)					
avg	9.38	39.2	0.648	0.780	19.8
max	9.40	39.3	0.649	0.783	20.0

Table 2. I - V results for a reference group and a group with improved rear surface. Both groups had a stencilled front metal grid.

Fig. 6 shows the implied V_{oc} values of cells without metallization for three different phosphorus BSF doping profiles with increasing sheet resistivity R_{sheet}

(lower doping). The rest of the processing is the same. For BSF profile 3, a gain of implied V_{oc} of more than 15mV is observed over the standard BSF profile 1.

On the cell level, the best BSF doping profile from the test was compared to the standard BSF profile. Fig. 7 shows the J_{sc} and V_{oc} data of the different experiment runs (again executed on n-type Cz from different suppliers). For each run (distinguished by different symbols), a standard group (blue) and a group with an improved rear surface (red) were processed. The gain in $J_{sc} \cdot V_{oc}$ is around 3% relative, which was clearly reproducible for each run and independent of the material properties.

For each of the experiments, a gain of 8 to 10mV was observed for the cells with improved BSF profile; this increase in V_{oc} can be explained by the improved rear-surface passivation. The difference in V_{oc} improvements between cells with metallization (~8–10mV) and without metallization (15mV) can be explained by the contact recombination below the rear metal contacts. To optimize the rear surface further, reducing the metal fraction is clearly one option. Another possibility is improving the surface passivation itself by changing or adjusting the deposited dielectric layer.

In Fig. 7 an increase in J_{sc} is observed for the improved BSF. This is partly due to improved rear-surface passivation, but also results from the reduction in free-carrier absorption. The measured front reflection of cells with three different BSF profiles is shown in Fig. 8: BSF-2 and BSF-3 show enhanced reflection above 1000nm. For the improved phosphorous profiles of BSF-2 and BSF-3, the free-carrier absorption is reduced and therefore more light is reflected from the rear, causing an increase in J_{sc} .

The I - V measurement results for one of the experiments aimed at improving BSF diffusion are shown in Table 2. In this experiment both groups had an improved front-side metallization using the stencil print as described earlier. This resulted in an average efficiency of 19.4% (19.5% maximum) for group 1 with a standard BSE. Group 2, with an improved rear surface, yielded significantly improved voltage V_{oc} and current J_{sc} . Even though the FF is somewhat lower, an overall efficiency gain of 0.4% absolute is realized, leading to an average efficiency of 19.8%. A maximum efficiency of 20%, measured in-house, has been achieved.

As the cell is bifacial, the internal quantum efficiency (IQE) can be determined for both front and rear sides. The IQE graphs from the front side (Fig. 9a) show that the long wavelength response has improved, while with rear-side illumination (Fig. 9b) both long and short wavelength responses have improved. This is a clear indication of reduced rear-surface recombination and improved rear internal reflection, as was also confirmed by PCID fits on these measurements.

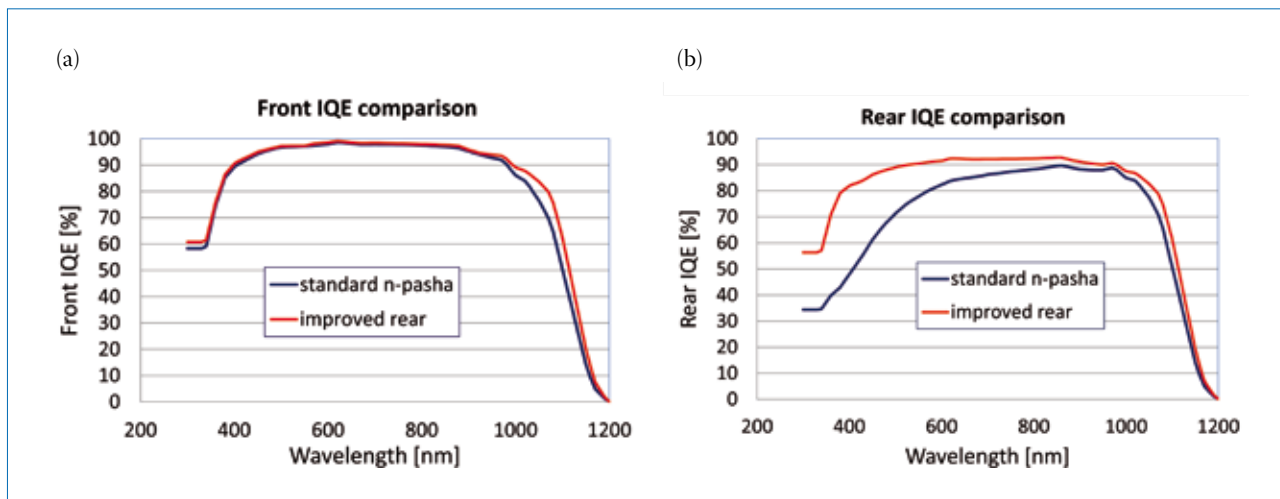


Figure 9. (a) Internal quantum efficiency (IQE) measured from (a) the front, and (b) the rear. The difference for cells with an improved rear surface is clear in both graphs.

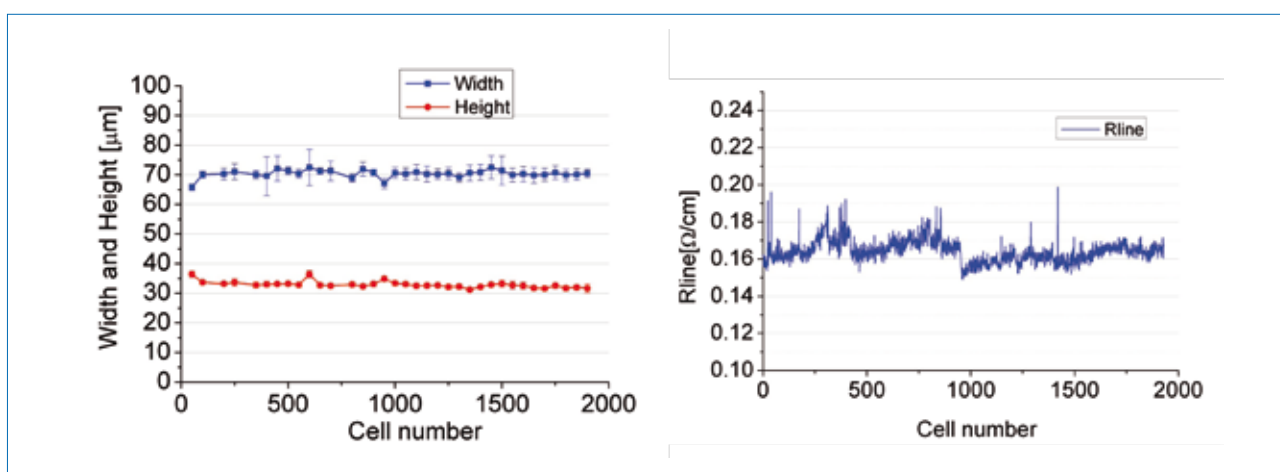


Figure 10. Line resistance and line width and height of the stencilled fingers as a function of cell number for 2000 industrially processed solar cells.

A two-dimensional model is currently being built to simulate the I - V and IQE characteristics of n-pasha cells, on the basis of input parameters such as diffusion profiles, surface recombination velocities and bulk lifetime. Use of this model will allow the current n-pasha cells to be accurately simulated, as well as providing insight into how the efficiency might be improved even further.

Industrial application of the new process steps

In order to test the industrial application of the two-step stencil printing concept, a limited endurance test was conducted in a production environment. The standard two-step stencil process as presented by Heurtault et al. [19] was selected for this test.

Width [μm]	Height [μm]	R_{line} [mΩ/cm]
70.4±1.3	32.9±1.1	164±11

Table 3. Average geometrical and electrical results for stencilled fingers.

Approximately 2000 cells were printed using one stencil, and one screen was used to print the busbars. Testing was done in two subsequent runs; the stencil was cleaned after the first half of the test and reused in the next. Line resistance was monitored for all cells, and line width and height for every 50 cells, with width and height values being averaged from nine measurement points per cell. The results are shown in Fig. 10 and Table 3.

Throughout the test, the geometry of the lines remained within specifications, with a very low standard deviation; the line resistance was stable, staying below 200mΩ/cm. The stencil did not show any signs of wear or tear and kept its integrity during the entire test. This first trial is promising as regards the robustness of the stencil process, but a more extensive test will be necessary to quantify the lifetime of the stencil and the print quality on longer runs.

The improved BSF has not yet been tested on very large quantities of cells. However, as can be seen from Fig. 7, the process has yielded quite stable results on different selections of materials, with similar increases in J_{sc} and V_{oc} in all cases.

Further improvements

The next steps towards achieving efficiencies higher than 20% for n-type pasha cells will involve:

- Decreasing the rear-surface metallization. This will not only improve the efficiency by decreasing the drop in V_{oc} from the implied V_{oc} values, but also improve the cost of ownership by decreasing silver consumption.
- Optimizing rear-side passivation layers, which is expected to further increase the benefit in J_{sc} and V_{oc} from the tuned BSF.
- Improving the emitter profile and optimizing further the front-surface passivation. With better rear-surface and reduced front-side metallization, improvements to the front side will have a beneficial impact on efficiency.
- Investigating a different cell architecture. One way to further reduce the front metal coverage, and thereby improve I_{sc} and V_{oc} without FF loss, is to use a metal-wrap-through (MWT) cell concept [20]. Another advantage of this

cell concept is the smaller losses in FF when the cells are interconnected into a module. Yingli and ECN have published results of their ongoing development in this area [21,22].

“Combining the use of stencilled fingers and an optimized BSF diffusion has made it possible to achieve an efficiency of 20% for n-pasha cells manufactured using industrial processes.”

Conclusions

This paper has presented two improved processes that have been recently tested on ECN's n-pasha cell concept. By using stencilled fingers, the front-side metallization has been reduced by 2%, resulting in an improvement of around 0.4% absolute in efficiency. Furthermore, the BSF diffusion has been optimized in terms of passivation and optics, also resulting in a gain of 0.4% absolute in efficiency. Combining the use of stencilled fingers and an optimized BSF diffusion has made it possible to achieve an efficiency of 20% for n-pasha cells manufactured using industrial processes.

The two-step stencil process has been successfully tested on a large number of cells in a production environment. The performance remained stable, and the stencil did not show any signs of wear, demonstrating its industrial applicability.

Acknowledgements

T. Burgers, B. Geerligs, K. Tool, A. Carr, A. Gutjahr, D. Saynova, B. Heurtault, J. Anker, M. Koppes, X. Jingfeng, L. Gaofei, X. Zhuo, W. Hongfang, H. Zhiyan and P. Venema are gratefully acknowledged for their contributions to this paper.

References

- [1] Hirshman, W.P. 2009, “Little smiles on long faces (cell production 2008: survey)”, *Photon Inter.* (March), pp. 170–206.
- [2] Sunpower [details online at <http://us.sunpowercorp.com>].
- [3] Sanyo [details online at <http://www.sanyo.com/solar>].
- [4] Cousins, P.J. et al. 2011, “Generation 3: Improved performance at lower cost”, *Proc. 35th IEEE PVSC*, Honolulu, Hawaii, USA, pp. 275–278.
- [5] Burgers A.R. et al. 2011, “19.5% efficient n-type Si solar cells made in production”, *Proc. 26th EU PVSEC*, Hamburg, Germany.
- [6] Saitoh, T. et al. 2000, “Suppression of light-induced degradation of minority carrier lifetimes in low-resistivity Cz-silicon wafers and solar cells”, *Proc. 16th EU PVSEC*, Glasgow, UK, pp. 1206–1209.
- [7] Das, A. & Rohatgi, A. 2011, “The impact of cell design on light induced degradation in p-type silicon solar cells”, *Proc. 37th IEEE PVSC*, Seattle, Washington, USA.
- [8] Schmidt, J. & Hezel, R. 2002, “Light-induced degradation in Cz silicon solar cells: Fundamental understanding and strategies for its avoidance”, *Proc. 12th Worksh. Cryst. Si. Sol. Cell Mater. & Process.*, Golden, Colorado, USA.
- [9] Macdonald, D. & Geerligs, L.J. 2004, “Recombination activity of interstitial iron and other transition metal point defects in p- and n-type crystalline silicon”, *Appl. Phys. Lett.*, Vol. 85, pp. 4061–4063.
- [10] Cuevas, A. et al. 2002, “Millisecond minority carrier lifetimes in n-type multicrystalline silicon”, *Appl. Phys. Lett.*, Vol. 81, pp. 4952–4954.
- [11] Altermatt, P.P. et al. 2006, “The surface recombination velocity at boron-doped emitters: Comparison between various passivation techniques”, *Proc. 21st EU PVSEC*, Dresden, Germany, pp. 647–650.
- [12] Hoex, B. et al. 2007, “Excellent passivation of highly doped p-type Si surfaces by the negative-charge-dielectric Al_2O_3 ”, *Appl. Phys. Lett.*, Vol. 91, p. 112107.
- [13] Hoex, B. et al. 2008, “On the c-Si surface passivation mechanism by the negative-charge-dielectric Al_2O_3 ”, *J. Appl. Phys.*, Vol. 104, p. 113703.
- [14] Mihaleitchi, V.D. et al. 2008, “Nitric acid pretreatment for the passivation of boron emitters for n-type base silicon solar cells”, *Appl. Phys. Lett.*, Vol. 92, p. 63510.
- [15] Mihaleitchi, V.D. et al. 2010, “Screen-printed n-type silicon solar cells for industrial application”, *Proc. 25th EU PVSEC*, Valencia, Spain, pp. 1446–1448.
- [16] Komatsu, Y. et al. 2009, “Homogeneous p+ emitter diffused using boron tribromide for record 16.4% screen-printed large area n-type mc-Si solar cell”, *Solar Energy Mater. & Solar Cells*, Vol. 93, pp. 750–752.
- [17] Naber, R.C.G. 2009, “ECN n-type silicon solar cell technology: An industrial process that yields 18.5%”, *Proc. 34th IEEE PVSC*, Philadelphia, Pennsylvania, USA.
- [18] Weeber A.W. 2009, “Status of n-type solar cells for low-cost industrial production”, *Proc. 24th EU PVSEC*, Hamburg, Germany.
- [19] Heurtault, B. & Hoonstra, J. 2010, “Towards industrial application of stencil printing for crystalline silicon solar cells”, *Proc. 25th EU PVSEC*, Valencia, Spain.
- [20] Weeber, A.W. 2006, “17% cell efficiencies on large back-contacted multi-crystalline silicon solar cells”, *Proc. 21st EU PVSEC*, Dresden, Germany.
- [21] Guillevin, N. et al. 2010, “High efficiency n-type metal wrap through Si solar cells for low-cost industrial production”, *Proc. 25th EU PVSEC*, Valencia, Spain, pp. 1429–1431.
- [22] Guillevin, N. et al. 2011, “Development towards 20% efficient n-type Si MWT solar cells for low-cost industrial production”, *Proc. 26th EU PVSEC*, Hamburg, Germany.

Enquiries

ECN Solar Energy
P.O. Box 1
NL-1755 ZG Petten
The Netherlands
Tel: +31 224 56 4959
Fax: +31 224 56 8214
Email: romijn@ecn.nl

Yingli Solar
3399 Chaoyang North Street
Baoding
China

Tempress Systems BV
Radeweg 31
8171 Vaassen
The Netherlands